Electronic Supplementary Material (ESI) for Nanoscale.

Electronic Supplemental Information for

$Au_3(\mu_3\text{-}S)(0e)$ Elementary Block: New Insights into Ligated Gold Clusters with μ_3-Sulfido Motifs

Wen Wu Xu, Xiao Cheng Zeng, Yi Gao

Correspondence Email: xzeng1@unl.edu, gaoyi@sinap.ac.cn

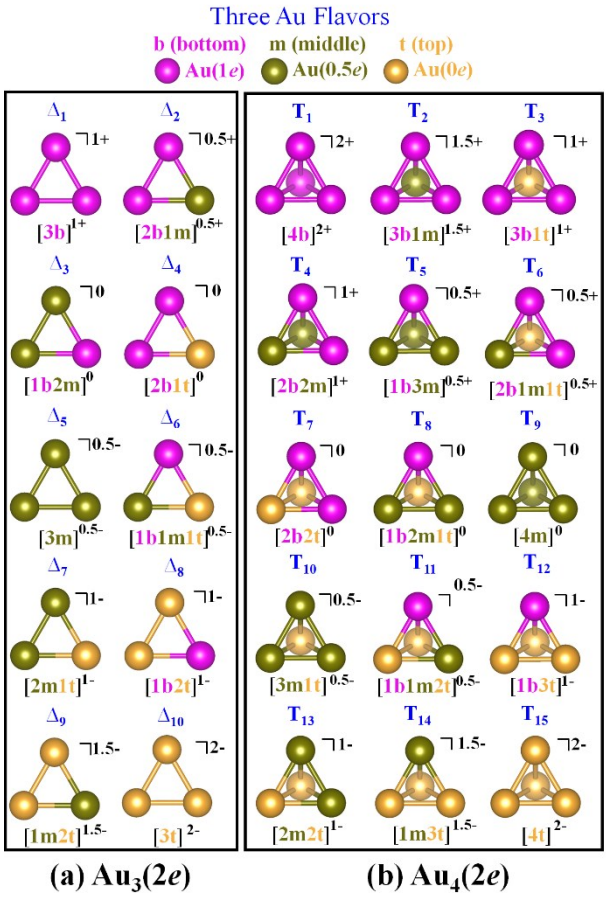

Figure S1. (a) Ten variants ($\Delta_1 - \Delta_{10}$) of valence states for the triangular elementary block $Au_3(2e)$ and (b) 15 variants ($T_1 - T_{15}$) of valence states for the tetrahedral elementary block $Au_4(2e)$. b(bottom), m(middle), and t(top) denote bottom flavor (Au(1*e*)), middle flavor (Au(0.5*e*)), and top flavor (Au(0*e*)), respectively. Color code: Au(1*e*) – magenta ("bottom flavor"); Au(0.5*e*) – dark yellow ("middle flavor"); Au(0*e*) – yellow ("top flavor").

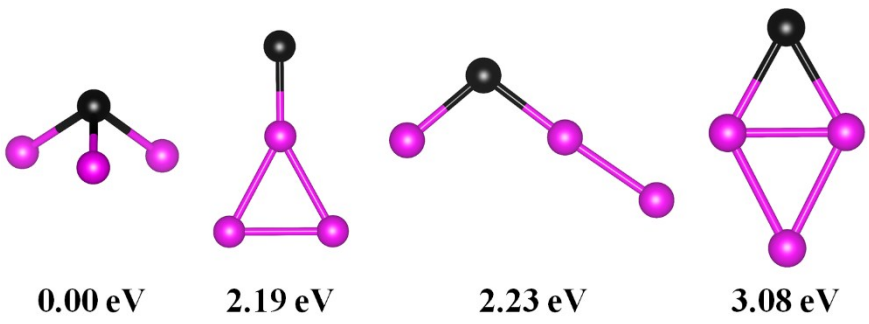

Figure S2. Four optimized isomers of Au_3S with zero valence electron as well as their relative energies. Color code: Au – magenta; S – black.

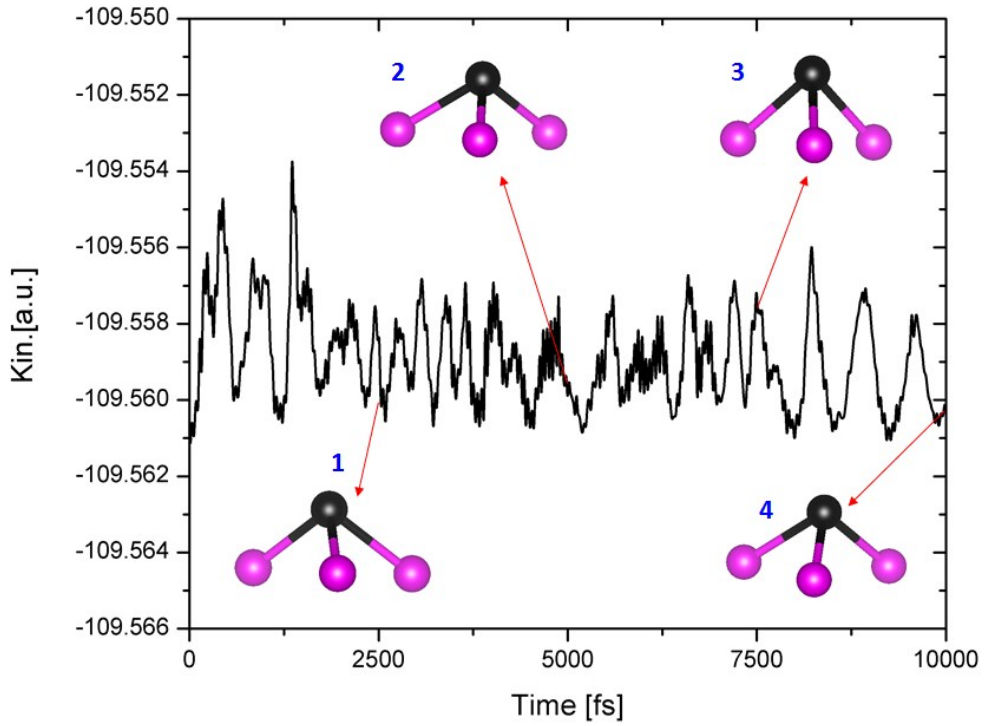

Figure S3. Computed kinetic energy (Kin) vs simulation time in an *ab initio* molecular dynamics simulations of $Au_3(\mu_3\text{-S})(0e)$ at 355 K. 1, 2, 3, and 4 correspond to the structure at 2.5, 5, 7.5, and 10 ps, respectively. Color code: Au – magenta; μ_3-S – black.

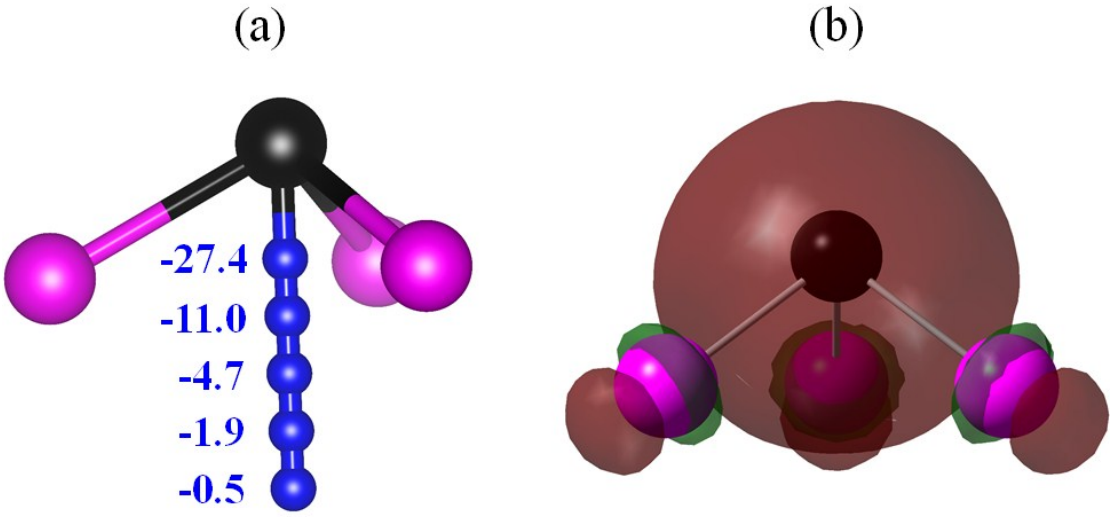

Figure S4. Computed nucleus-independent chemical shift (NICS) values (a) and delocalized orbital (b) of $Au_3(\mu_3\text{-S})(0e)$. Color code: Au – magenta; μ_3-S – black; dummy atom – blue.

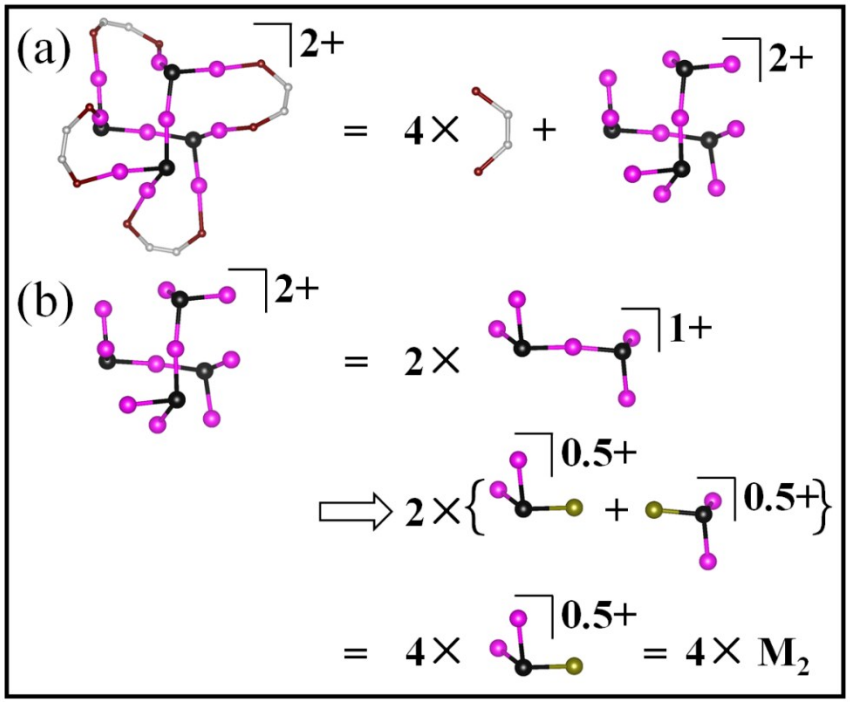

Figure S5. Structural decomposition of $[Au_{10}(\mu\text{-}cis\text{-dppee})_4(\mu_3\text{-S})4]^{2+}$ (dppee = 1,2-bis(diphenylphosphino)ethene) (a and b). Color code: Au(1*e*) – magenta ("bottom flavor"); Au(0.5*e*) – dark yellow ("middle flavor"); μ_3-S – black; PR_3 – wine; C – gray. The Ph and H groups are omitted for clarity.

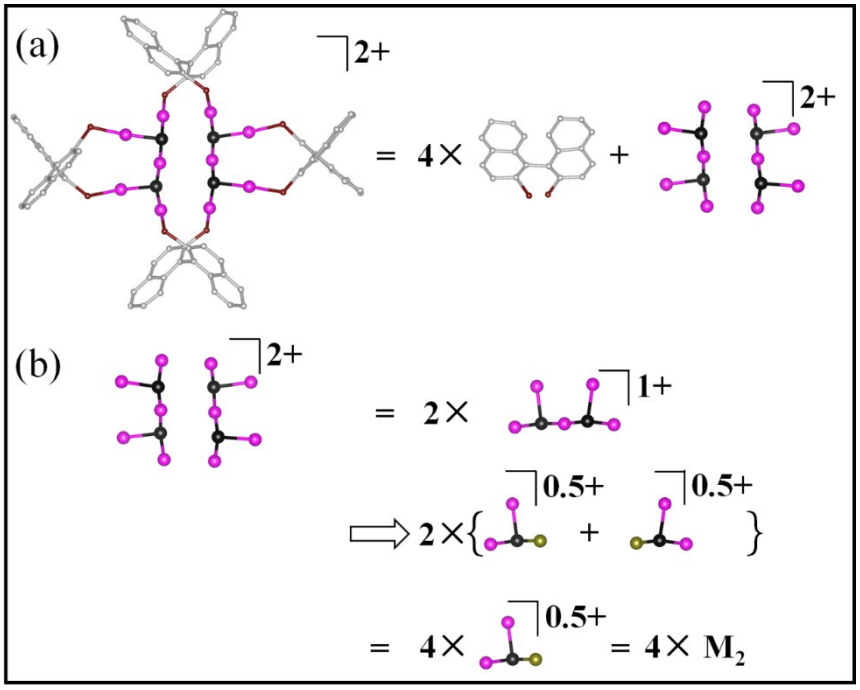

Figure S6. Structural decomposition of $[Au_{10}(R\text{-BINAP})_4(\mu_3\text{-S})_4]^{2+}$ (BINAP = 2,2'-bis(diphenylphosphino)-1,1'-binaphthyl) (a and b). Color code: Au(1*e*) – magenta ("bottom flavor"); Au(0.5*e*) – dark yellow ("middle flavor"); μ_3-S – black; PR_3 – wine; C – gray. The Ph and H groups are omitted for clarity.

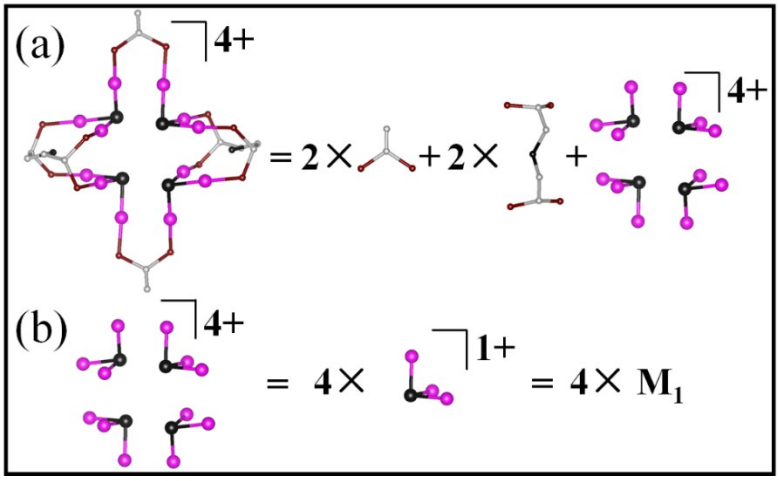

Figure S7. Structural decomposition of $[Au_{12}(\mu\text{-vdpp})_2(\mu\text{-dppes})_2(\mu_3\text{-S})_4]^{4+}$ (vdpp = vinylidenebis(diphenylphosphine) and dppes = bis-(2,2-bis(diphenylphosphino)ethyl)sulfane) (a and b). Color code: Au(1*e*) – magenta ("bottom flavor"); μ_3-S – black; PR_3 – wine; C – gray. The Ph and H groups are omitted for clarity.

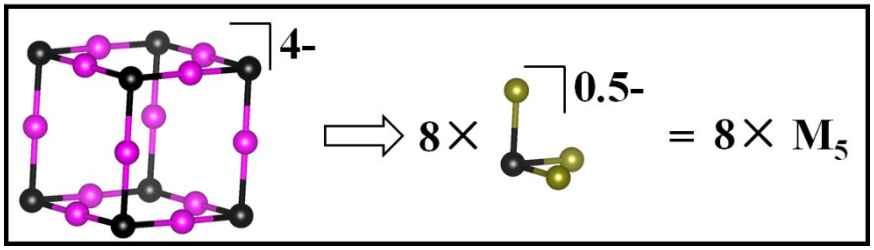

Figure S8. Structural decomposition of $[Au_{12}(\mu_3\text{-S})_8]^{4-}$. Color code: Au(1*e*) – magenta ("bottom flavor"); Au(0.5*e*) – dark yellow ("middle flavor"); μ_3-S – black; PR_3 – wine; C – gray.

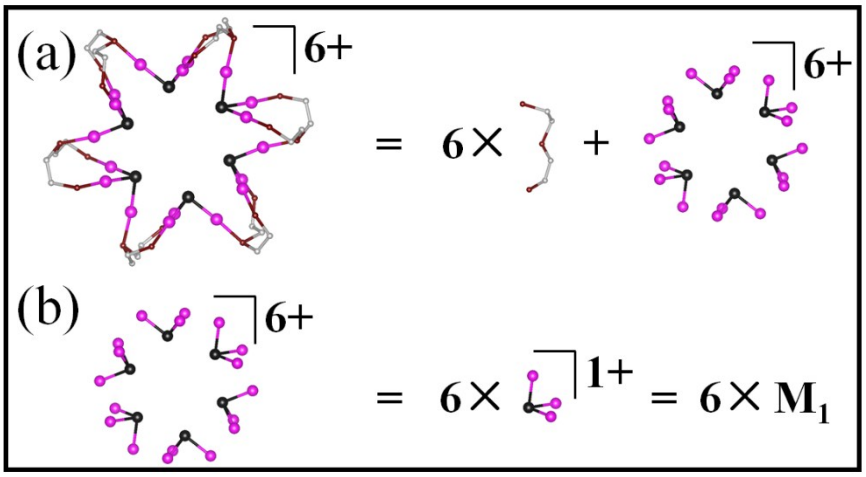

Figure S9. Structural decomposition of $[Au_{18}(\mu\text{-dpepp})_6(\mu_3\text{-S})_6]^{6+}$ (dpepp = bis(2-diphenylphosphinoethyl)phenylphosphine) (a and b). Color code: Au(1*e*) – magenta ("bottom flavor"); μ_3-S – black; PR_3 – wine; C – gray. The Ph and H groups are omitted for clarity.

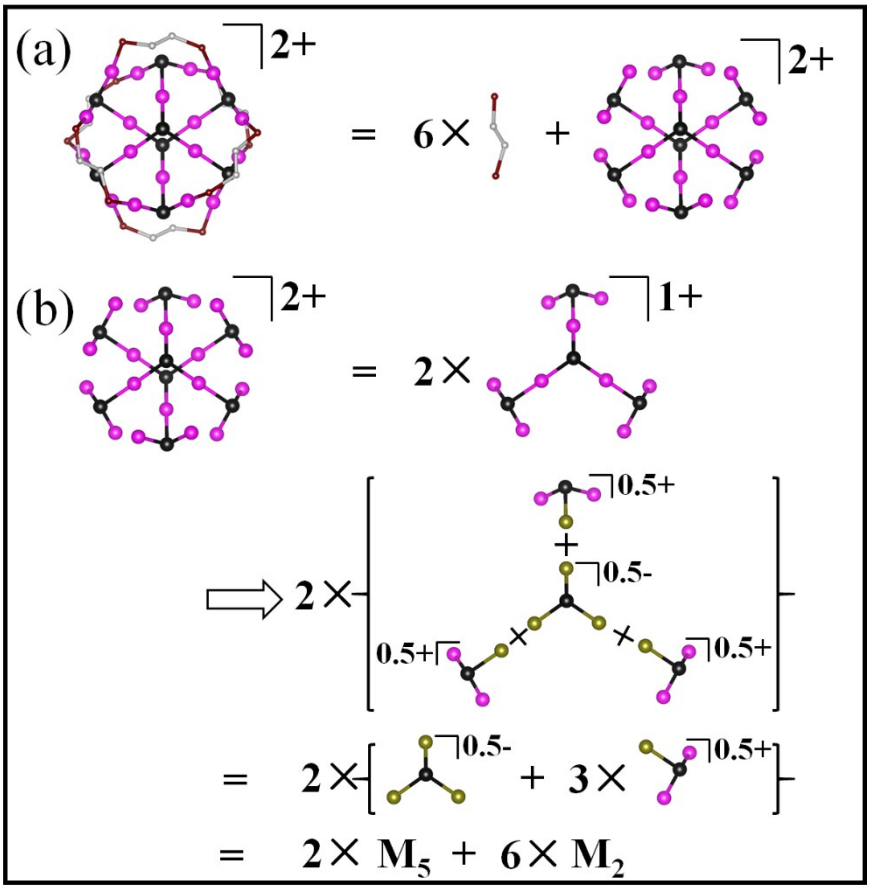

Figure S10. Structural decomposition of $[Au_{18}(\mu\text{-}trans\text{-}dppee)_6(\mu_3\text{-}S)_8]^{2+}$ (dppee = 1,2-bis(diphenylphosphino)ethene)) (a and b). Color code: Au(1*e*) – magenta ("bottom flavor"); Au(0.5*e*) – dark yellow ("middle flavor"); μ_3-S – black; PR_3 – wine; C – gray. The Ph and H groups are omitted for clarity.

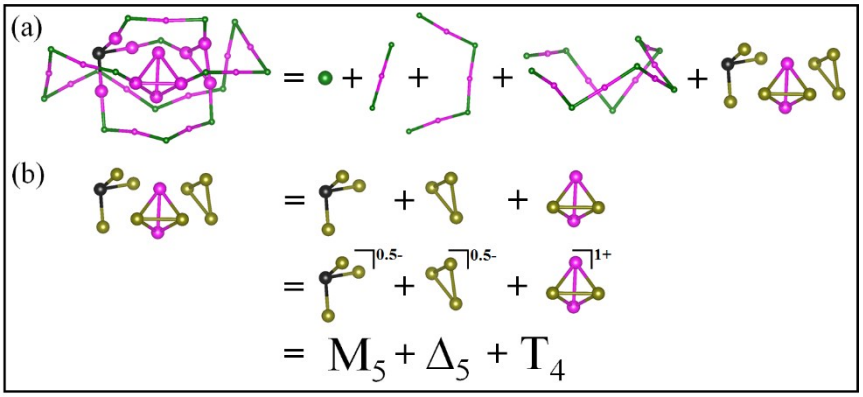

Figure S11. Structural decomposition of $Au_{21}(\mu_3\text{-}S)(SR)_{15}$ (a and b). Color code: Au(1*e*) – magenta ("bottom flavor"); Au(0.5*e*) – dark yellow ("middle flavor"); μ_3-S – black; SR – dark green. The R groups are omitted for clarity.

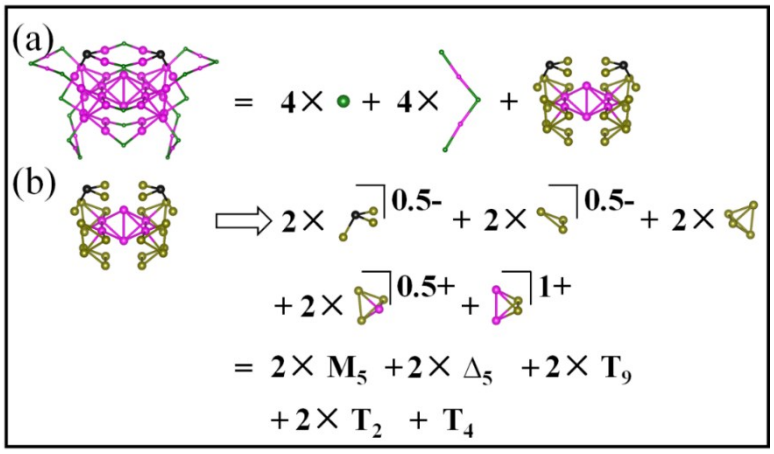

Figure S12. Structural decomposition of $Au_{38}(\mu_3\text{-}S)_2(SR)_{20}$ (a and b). Color code: Au(1*e*) – magenta ("bottom flavor"); Au(0.5*e*) – dark yellow ("middle flavor"); μ_3-S – black; SR – dark green. The R groups are omitted for clarity.

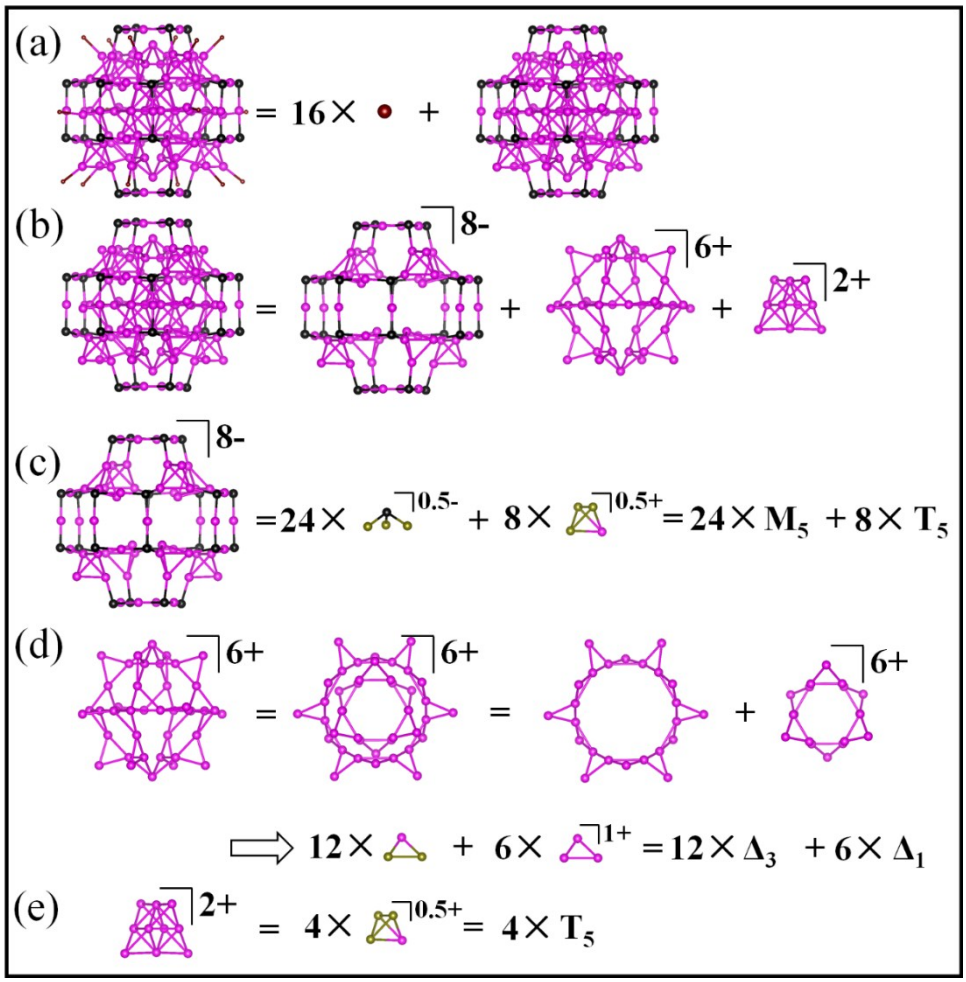

Figure S13. Structural decomposition of $Au_{108}(\mu_3\text{-}S)_{24}(PR_3)_{16}$ (a, b, c, d, and e). Color code: Au(1*e*) – magenta ("bottom flavor"); Au(0.5*e*) – dark yellow ("middle flavor"); μ_3-S – black; PR_3 – wine. The Ph groups are omitted for clarity.

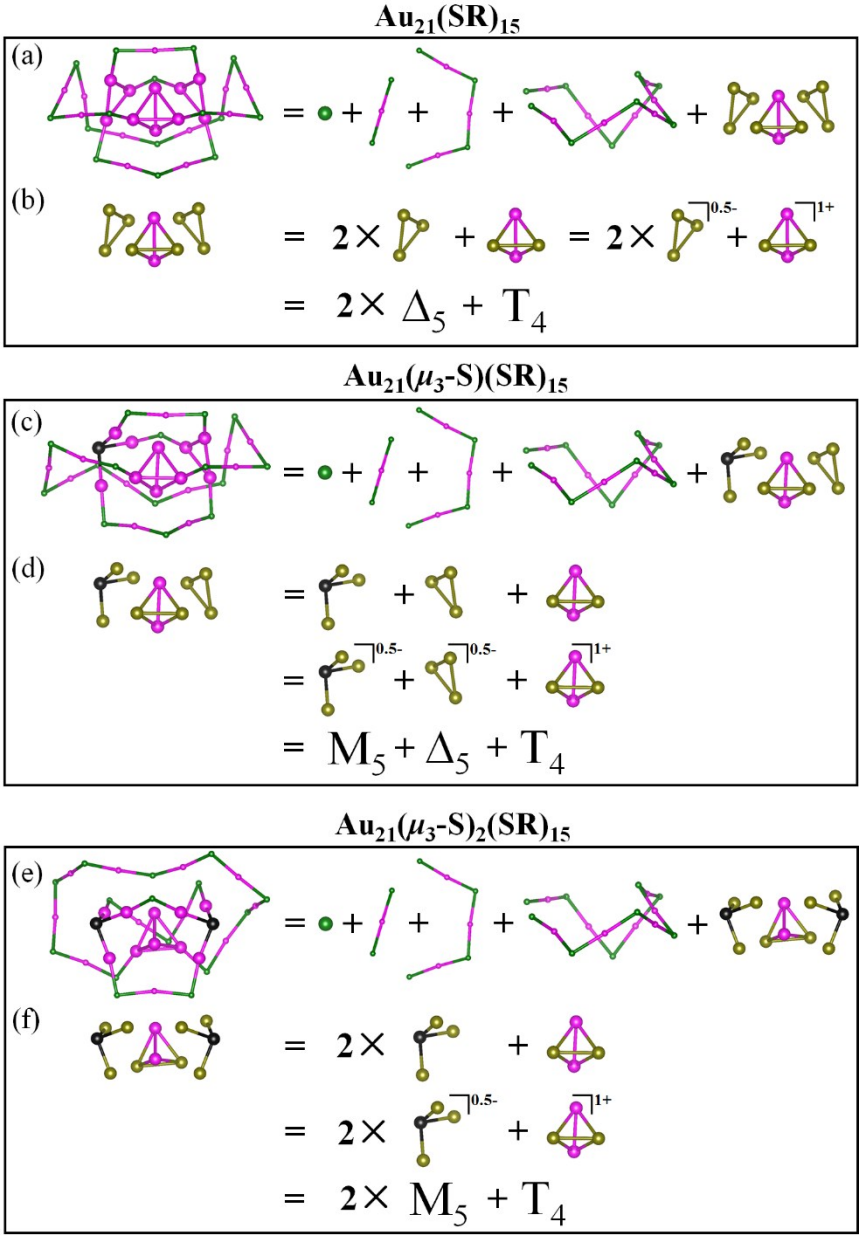

Figure S14. Structural decomposition of $Au_{21}(SR)_{15}$ (a and b), $Au_{21}(\mu_3\text{-S})(SR)_{15}$ (c and d), and $Au_{21}(\mu_3\text{-S})_2(SR)_{15}$ (e and f). Color code: Au(1*e*) – magenta ("bottom flavor"); Au(0.5*e*) – dark yellow ("middle flavor"); SR – dark green; μ_3-S – black. The R groups are omitted for clarity.

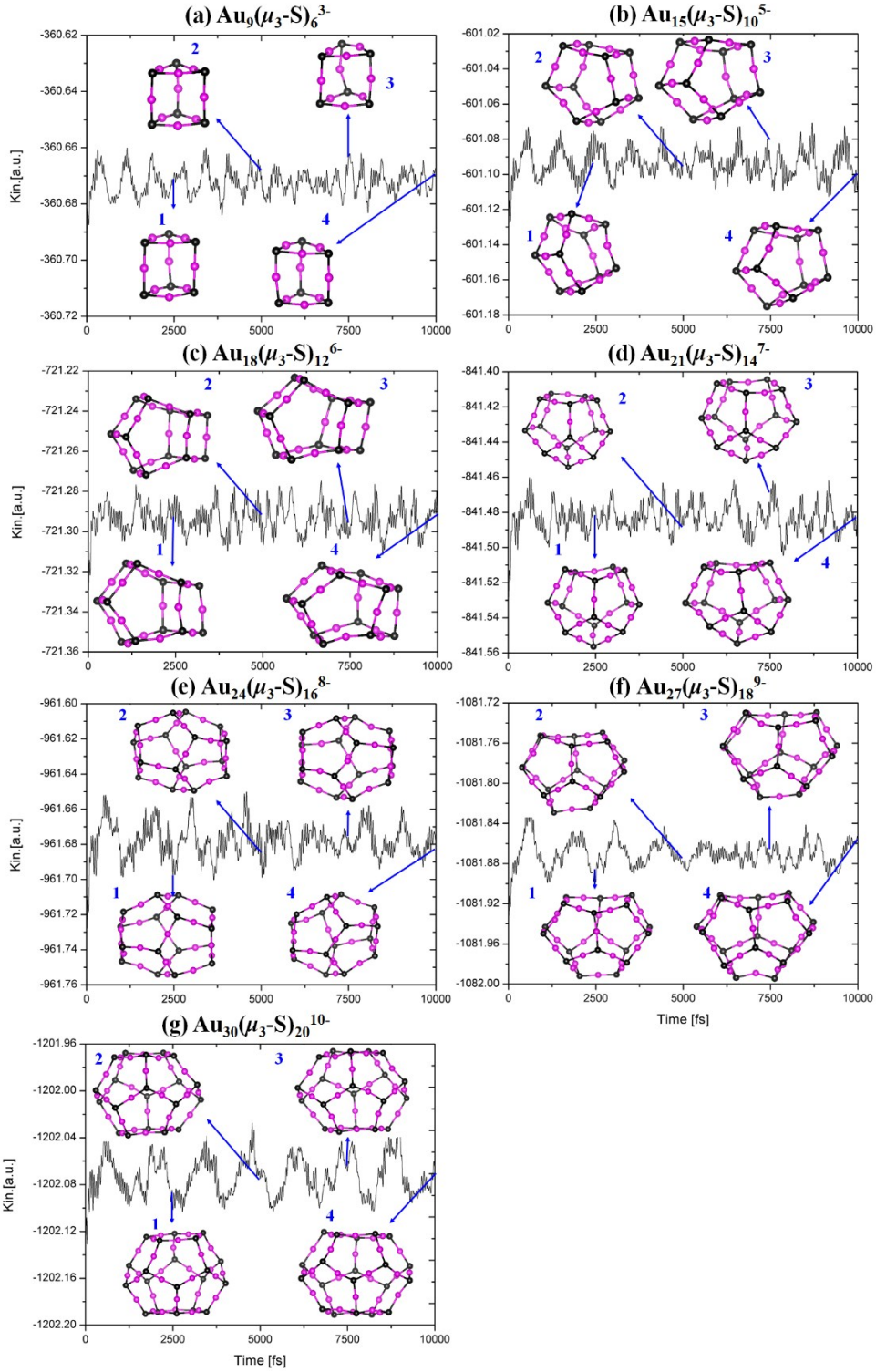

Figure S15. Computed kinetic energy (Kin) vs simulation time in *ab initio* molecular dynamics simulations of $Au_9(\mu_3\text{-}S)_6^{3-}$ (a), $Au_{15}(\mu_3\text{-}S)_{10}^{5-}$ (b), $Au_{18}(\mu_3\text{-}S)_{12}^{6-}$ (c), $Au_{21}(\mu_3\text{-}S)_{14}^{7-}$ (d), $Au_{24}(\mu_3\text{-}S)_{16}^{8-}$ (e), $Au_{27}(\mu_3\text{-}S)_{18}^{9-}$ (f), and $Au_{30}(\mu_3\text{-}S)_{20}^{10-}$ (g), at 355 K. 1, 2, 3, and 4 correspond to the structure at 2.5, 5, 7.5, and 10 ps, respectively. Color code: Au – magenta; μ_3-S – black.

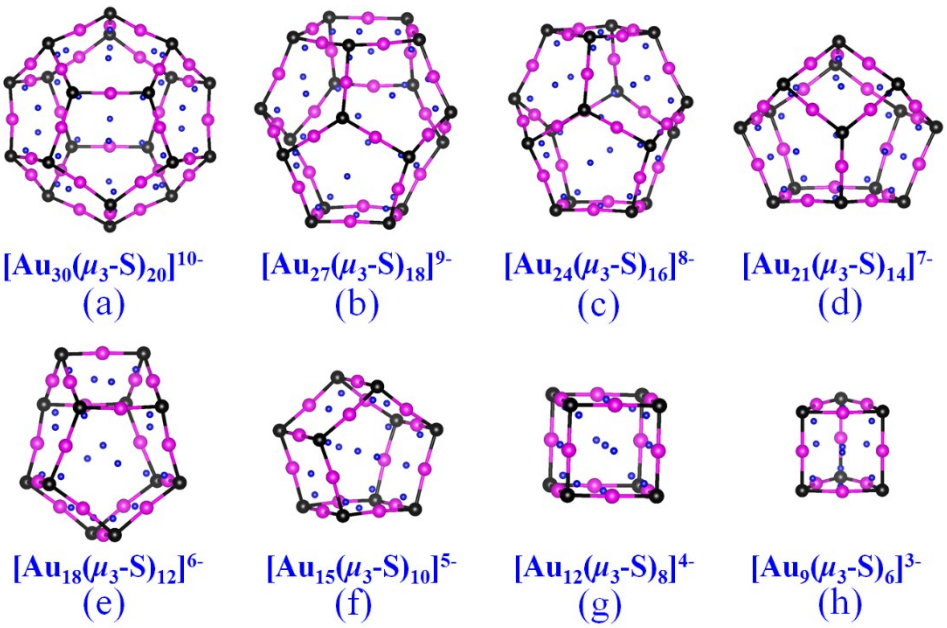

Figure S16. Computed nucleus-independent chemical shift (NICS) grids for $Au_9(\mu_3\text{-}S)_6^{3-}$ (a), $Au_{12}(\mu_3\text{-}S)_8^{4-}$ (b), $Au_{15}(\mu_3\text{-}S)_{10}^{5-}$ (c), $Au_{18}(\mu_3\text{-}S)_{12}^{6-}$ (d), $Au_{21}(\mu_3\text{-}S)_{14}^{7-}$ (e), $Au_{24}(\mu_3\text{-}S)_{16}^{8-}$ (f), $Au_{27}(\mu_3\text{-}S)_{18}^{9-}$ (g), and $Au_{30}(\mu_3\text{-}S)_{20}^{10-}$ (h). Color code: Au – magenta; μ_3-S – black; dummy atom – blue.

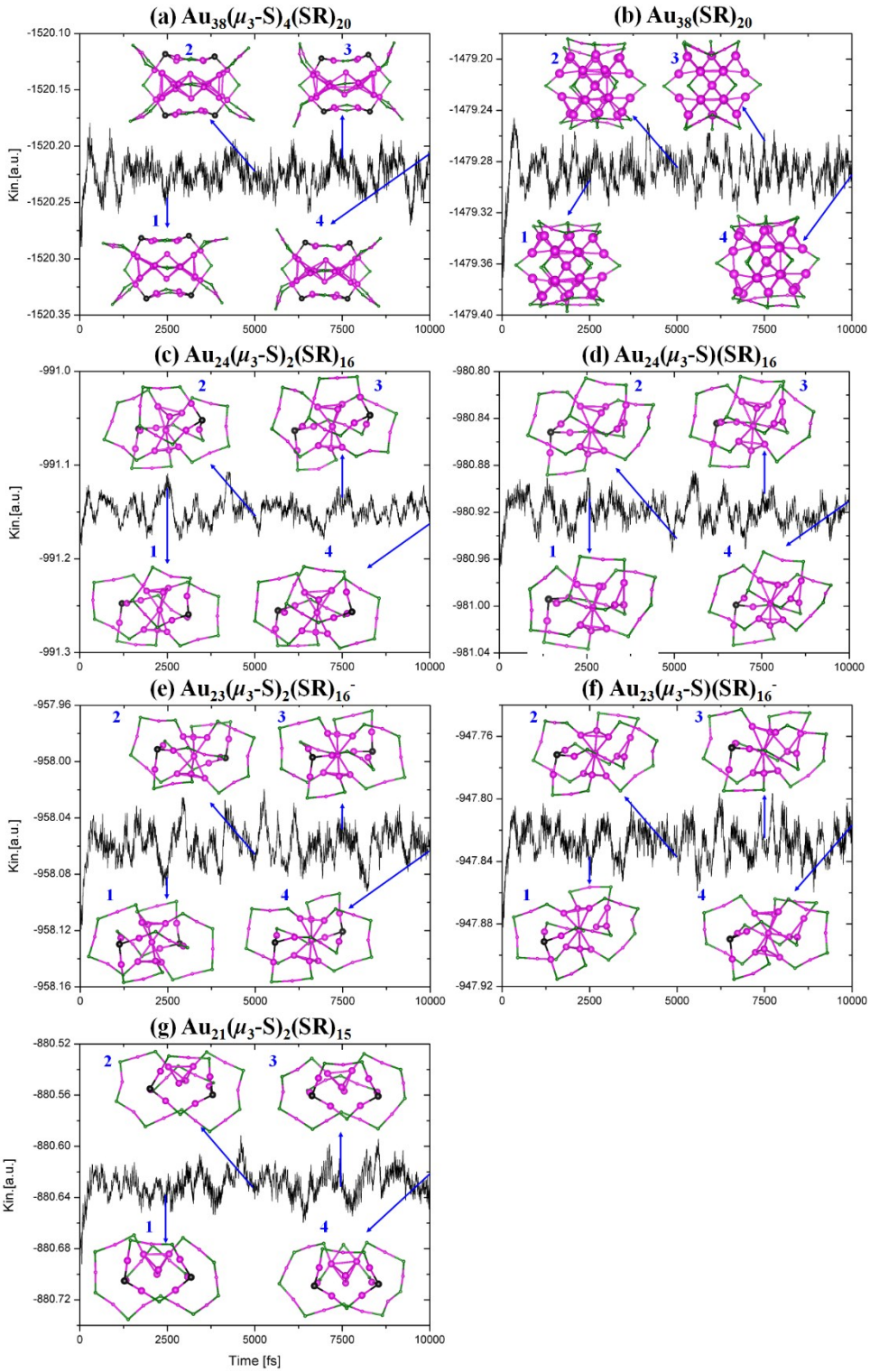

Figure S17. Computed kinetic energy (Kin) vs simulation time in *ab initio* molecular dynamics simulations of $Au_{38}(\mu_3\text{-}S)_4(SR)_{20}$ (a), $Au_{38}(SR)_{20}$ (b), $Au_{24}(\mu_3\text{-}S)_2(SR)_{16}$ (c), $Au_{24}(\mu_3\text{-}S)(SR)_{16}$ (d), $Au_{23}(\mu_3\text{-}S)_2(SR)_{16}^-$ (e), $Au_{23}(\mu_3\text{-}S)(SR)_{16}^-$ (f), and $Au_{21}(\mu_3\text{-}S)_2(SR)_{15}$ (g) at 355 K. 1, 2, 3, and 4 correspond to the structure at 2.5, 5, 7.5, and 10 ps, respectively. Color code: Au – magenta; μ_3-S – black; SR – dark green. The R groups (H atoms) are omitted for clarity.

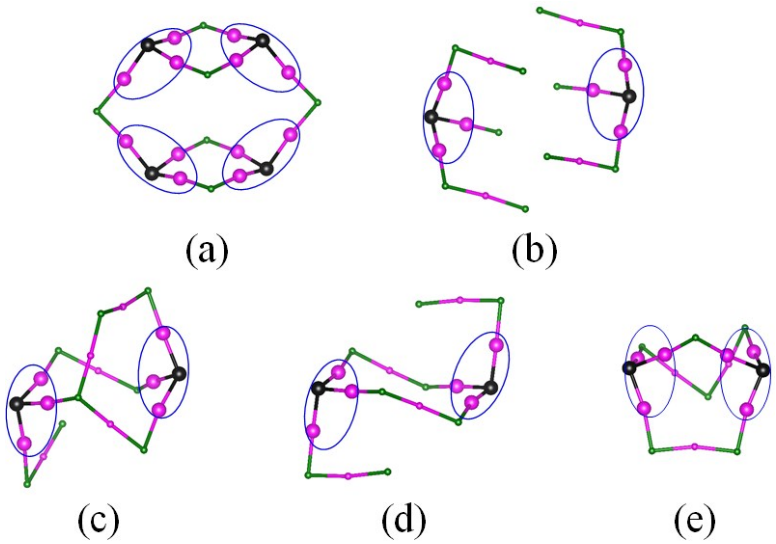

Figure S18. The network of protected ligands of $Au_{38}(\mu_3\text{-}S)_4(SR)_{20}$ (a), $Au_{30}(\mu_3\text{-}S)_2(SR)_{18}$ (b), $Au_{24}(\mu_3\text{-}S)_2(SR)_{16}$ (c), $Au_{23}(\mu_3\text{-}S)_2(SR)_{16}^-$ (d), and $Au_{21}(\mu_3\text{-}S)_2(SR)_{15}$ (e). The $Au_3(\mu_3\text{-}S)(0e)$ elementary blocks are highlighted by blue ovals. Color code: Au – magenta; μ_3-S – black; SR – dark green. The R groups are omitted for clarity.

Table S1 Total 19 crystallized structures whose gold cores are composed of the elementary blocks at various valence states.

Structures	Elementary blocks at various valence states
$[(AuPPh_3)_3(\mu_3\text{-}S)]^+$ [5]	M_1
$[(AuC_6F_5)_3(\mu_3\text{-}S)]^{2-}$ [6]	M_{10}
$[(AuCNC_7H_{13})_3(\mu_3\text{-}S)]^+$ [7]	M_1
$[Au_5(PPh_3)_4(\mu_3\text{-}S)_2]^+$ [8]	$2M_2$
$[Au_6\{\mu\text{-}Ph_2PN(p\text{-}CH_3C_6H_4)PPh_2\}_3(\mu_3\text{-}S)_2]^{2+}$ [9，10]	$2M_1$
$[Au_{10}(\mu\text{-}PNP)_4(\mu_3\text{-}S)_4]^{2+}$ [11]	$4M_2$
$[Au_{10}(R\text{-}BINAP)_2(S\text{-}BINAP)_2(\mu_3\text{-}S)_4]^{2+}$ [12]	$4M_2$
$[Au_{10}\{Ph_2PN(R)PPh_2\}_4(\mu_3\text{-}S)_4]^{2+}$ [10，13]	$4M_2$
$[Au_{10}(\mu\text{-}cis\text{-}dppee)_4(\mu_3\text{-}S)_4]^{2+}$ [14]	$4M_2$
$[Au_{10}(\mu\text{-}vdpp)_4(\mu_3\text{-}S)_4]^{2+}$ [15]	$4M_2$
$[Au_{10}(R\text{-}BINAP)_4(\mu_3\text{-}S)_4]^{2+}$ [12]	$4M_2$
$[Au_{12}(\mu\text{-}dppm)_6(\mu_3\text{-}S)_4]^{4+}$ [16]	$4M_1$
$[Au_{12}(\mu\text{-}vdpp)_2(\mu\text{-}dppes)_2(\mu_3\text{-}S)_4]^{4+}$ [15]	$4M_1$
$[Au_{12}(\mu_3\text{-}S)_8]^{4-}$ [17]	$8M_5$
$[Au_{18}(\mu\text{-}dpepp)_6(\mu_3\text{-}S)_6]^{6+}$ [18]	$6M_1$
$[Au_{18}(dppe)_6(\mu_3\text{-}S)_8]^{2+}$ [14]	$6M_2+2M_5$
$[Au_{18}(\mu\text{-}trans\text{-}dppee)_6(\mu_3\text{-}S)_8]^{2+}$ [19]	$6M_2+2M_5$
$Au_{21}(\mu_3\text{-}S)(SR)_{15}$ [22]	$M_5+\Delta_4+T_4$
$Au_{30}(\mu_3\text{-}S)(SR)_{18}$ [23]	$M_5+\Delta_5+2T_5+2T_9$
$Au_{38}(\mu_3\text{-}S)_2(SR)_{20}$ [24]	$2M_5+2\Delta_5+2T_2+T_4+2T_9$
$Au_{108}(\mu_3\text{-}S)_{24}(PR_3)_{16}$ [25]	$24M_5+6\Delta_1+12\Delta_3+12T_5$

Table S2. Details decomposition of $Au_{21}(SR)_{15}$, $Au_{21}(\mu_3\text{-}S)(SR)_{15}$, and $Au_{21}(\mu_3\text{-}S)_2(SR)_{15}$ clusters.

	Number of valence electrons	$Au_4(2e)$	$Au_3(2e)$	$Au_3(\mu_3\text{-}S)(0e)$
$Au_{21}(SR)_{15}$	$6e$	T_4	$2\Delta_5$	0
$Au_{21}(\mu_3\text{-}S)(SR)_{15}$	$4e$	T_4	Δ_5	M_5
$Au_{21}(\mu_3\text{-}S)_2(SR)_{15}$	$2e$	T_4	0	$2M_5$

Table S3. Calculated properties of 15 ligand-protected Au nanoclusters. The formation energies are computed based on the formula $Au_m(SR)_n + q(\mu_3\text{-}S) = Au_m(\mu_3\text{-}S)_q(SR)_n$ (q = 1, 2, and 4). * denotes the predicted structure by removing or adding the μ_3-S atoms.

	HOMO-LUMO gap/eV	Formation energy/eV	Lowest/highest vibrational frequency/cm^{-1}
$Au_{38}(SR)_{20}^*$	1.03	0	11.2/2638.3
$Au_{38}(\mu_3\text{-}S)_2(SR)_{20}$	1.39	–6.56	10.9/2635.3
$Au_{38}(\mu_3\text{-}S)_4(SR)_{20}^*$	1.20	–11.97	8.5/2629.5
$Au_{30}(SR)_{18}$	1.22	0	8.4/2635.2
$Au_{30}(\mu_3\text{-}S)(SR)_{18}$	1.17	–3.16	8.8/2635.6
$Au_{30}(\mu_3\text{-}S)_2(SR)_{18}^*$	1.39	–6.38	8.7/2635.2
$Au_{24}(SR)_{16}$	1.22	0	8.1/2635.7
$Au_{24}(\mu_3\text{-}S)(SR)_{16}^*$	1.39	–2.89	7.1/2635.2
$Au_{24}(\mu_3\text{-}S)_2(SR)_{16}^*$	1.50	–5.86	8.8/2634.2
$Au_{23}(SR)_{16}^-$	1.85	0	7.6/2639.1
$Au_{23}(\mu_3\text{-}S)(SR)_{16}^{-*}$	1.90	–3.17	7.4/2633.0
$Au_{23}(\mu_3\text{-}S)_2(SR)_{16}^{-*}$	2.04	–6.07	5.8/2632.7
$Au_{21}(SR)_{15}$	1.47	0	8.3/2638.6
$Au_{21}(\mu_3\text{-}S)(SR)_{15}$	1.50	–3.24	5.9/2628.9
$Au_{21}(\mu_3\text{-}S)_2(SR)_{15}^*$	1.55	–6.13	7.1/2634.8